Diffuse ferroelectric transition and relaxational dipolar freezing in $(Ba,Sr)TiO_3$

1995 J. Phys.: Condens. Matter 7 1441

(http://iopscience.iop.org/0953-8984/7/7/024)

J. Phys : Condens. Matter 7 (1995) 1441–1460. Printed in the UK

Diffuse ferroelectric transition and relaxational dipolar freezing in (Ba,Sr)TiO_3

V S Tiwari, Neelam Singh and Dhananjai Pandey
School of Materials Science and Technology, Banaras Hindu University, Varanasi–221005, India

Received 25 May 1994, in final form 7 September 1994

Abstract. The effect of Sr^{2+} substitution on the structure and dielectric behaviour of $BaTiO_3$ is reported. It is shown that the smearing of the variation of dielectric constant with temperature in such samples is not due to compositional inhomogeneities. Observation of relaxational dipolar freezing below the hump temperature indicates the similarity of diffuse ferroelectric transition and orientational glass behaviour.

1. Introduction

The low-frequency dielectric constant (ϵ') of $BaTiO_3$ is known to exhibit a sharp change around 130 °C due to a weakly first-order paraelectric to ferroelectric phase transition. On partial substitution of barium by strontium, the variation of ϵ' around T_c gets smeared out in both ceramic [1–4] as well as single-crystal [5–8] specimens. Similar smeared responses have been observed in several other dirty displacive ferroelectrics (DDF) [9] such as $Ba(Ti,Sn)O_3$ [10, 11], $Ba(Ti,Zr)O_3$ [12], $(Ba,Ca)TiO_3$ [13, 14], $Pb(Mg_{1/3}Nb_{2/3})O_3$ [10, 15] and $Pb(Sc_{1/2}Ta_{1/2})O_3$ [16, 17]. Unlike normal displacive ferroelectrics (NDF), the real (ϵ'_m) and imaginary (ϵ''_m) parts of the dielectric constant (relative permittivity) do not peak at the same temperature in DDF. Instead, the temperature T''_m corresponding to ϵ''_m is lower than T'_m for ϵ'_m. Further, ϵ' of DDF does not obey the Curie–Weiss law above T'_m but follows a modified temperature dependence $1/\epsilon' = 1/\epsilon'_m + (T - T'_m)^\gamma / C'$, where C' is a Curie–Weiss-like constant and γ is the critical exponent, which lies in range $1 < \gamma < 2$ [14, 18]. In addition, DDF exhibit characteristic dielectric dispersion in the radiofrequency range [10, 15].

The smeared-our ϵ' versus T response has generally been attributed [10, 15, 17] to the presence of microregions with local compositions varying from the average composition over length scales of 100 to 1000 Å. Different microregions in a macroscopic sample are assumed [17] to transform at different temperatures. Thus the transformation takes place over a wide range of temperature, the so-called 'Curie-range', leading to what is commonly termed a 'diffuse phase transition' (DPT) due to compositional fluctuations. However, it is known that, even in compositionally homogeneous systems, quenched random disorder may break the long-range polar order locally at the unit-cell level, leading to a smeared-out ϵ' versus T response [19]. For low concentrations, quenched disorder stabilizes the domain state while higher concentrations may lead to the dipolar glass state with characteristic dynamic response [19].

In the present work, we have investigated the effect of quenched random disorder due to strontium substitution at the barium site on the ferroelectric phase transition behaviour of $BaTiO_3$. Experimental evidence is advanced to show that the peak in the dielectric constant

0953-8984/95/071441+20$19.50

in $(Ba_{1-x}Sr_x)TiO_3$ is not due to a static phenomenon associated with the ferroelectric structural phase transition but is due to a relaxational glass transition. The structural change observed in x-ray diffraction (XRD) patterns is attributed to 'local symmetry breaking' leading to clusters of dipoles that undergo relaxational freezing below a frequency-dependent temperature T_m'.

2. Sample preparation and structural characterizations

In order to investigate the intrinsic behaviour of the $Ba_{1-x}Sr_xTiO_3$ system, the role of sample preparation and its proper characterization is most crucial. It is important to have samples free from microscopic segregation and clustering of Ba/Sr ions. We have concentrated on ceramic samples whose compositional homogeneity can be controlled using powders obtained by different synthesis routes. In the present work, (Ba,Sr)TiO_3 powders were prepared by two different routes: the conventional dry (D) route and a novel semi-wet (SW) route. The conventional dry route of synthesis involved solid-state thermochemical reaction in a mixture of $BaCO_3$, $SrCO_3$ and TiO_2. Since the mixing is only at a particulate level in the dry route, there will be regions with excess/deficient strontium concentrations. Uniform distribution of barium and strontium is not expected in this method since this will require very long diffusion distances of the order of a few tens of thousands of unit cells if the average reactant particle size is about 1 μm [20]. In the semi-wet route, we first prepare $Ba_{1-x}Sr_xCO_3$ solid solution precursors by chemical coprecipitation to ensure uniform distribution of Ba and Sr ions. The precursor carbonate solid solution is then mixed with TiO_2 for thermochemical reaction to yield $Ba_{1-x}Sr_xTiO_3$. In contrast to the conventional dry route, where the typical separations between barium and strontium ions are of the order of several tens of thousands of unit cells, these ions are only a few unit cells apart, irrespective of the size of the precursor particles, in the semi-wet route. This will naturally ensure uniform supply of barium and strontium in the correct ratio at the unit-cell level during the solid-state thermochemical reaction with TiO_2 particles, and hence a homogeneous distribution of barium and strontium ions in the final product.

The structural characterizations of the precursors and calcined powders were carried out using Cu Kα radiation on a Rigaku rotating-anode x-ray diffractometer operating at 6 kW.

2.1. Synthesis and characterization of $(Ba_{1-x}Sr_x)CO_3$ precursor

$Ba_{1-x}Sr_xCO_3$ precursors for $x = 0.04$, 0.08, 0.12, 0.16, 0.20, 0.25 and 0.30 were prepared by adding ammonium carbonate solution to $BaCl_2$ and $SrCl_2$ aqueous solutions mixed in desired molar ratios. The filtrates were checked for the absence of Ba^{2+} and Sr^{2+}, which confirmed the complete coprecipitation of Ba^{2+} and Sr^{2+} present in the starting solutions. Precipitates were thoroughly washed with distilled water to remove chloride ions and then dried in an oven.

Figure 1 shows x-ray diffractometer records of $Ba_{1-x}Sr_xCO_3$ for $x = 0.04$, 0.08, 0.12, 0.16, 0.20 and 0.30. All the diffraction lines in this figure could be indexed with respect to the orthorhombic aragonite structure of $BaCO_3$. The absence of the most intense line of $SrCO_3$ at $2\theta = 25.17°$ confirms that the precursor carbonates are solid solutions of $BaCO_3$ and $SrCO_3$. Table 1 lists the lattice parameters and unit-cell volumes of $Ba_{1-x}Sr_xCO_3$ calculated on the basis of the orthorhombic aragonite structure. The unit-cell volume decreases monotonically with increasing strontium content since the ionic size of Sr^{2+} is smaller than that of Ba^{2+}. This further confirms that Sr^{2+} has indeed entered into the $BaCO_3$ matrix. Since these solid solution precursors have been prepared by chemical

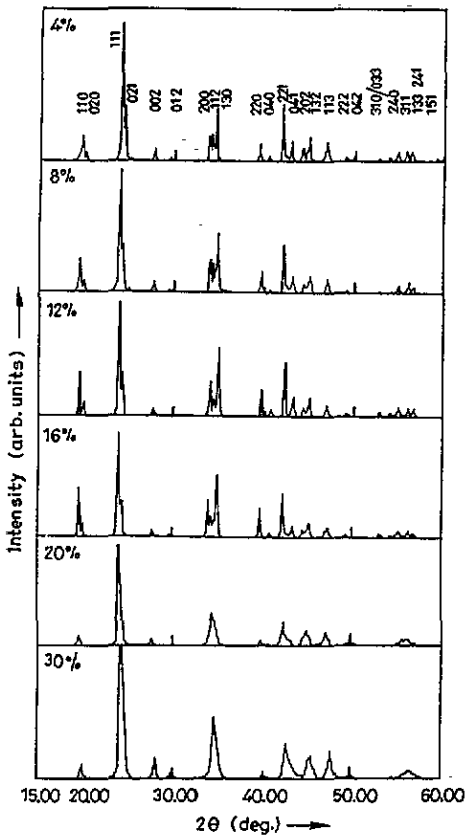

Figure 1. Powder diffractometer records of $Ba_{1-x}Sr_x$ CO_3 for $x = 0.04$, 0.08, 0.12, 0.16, 0.20 and 0.30.

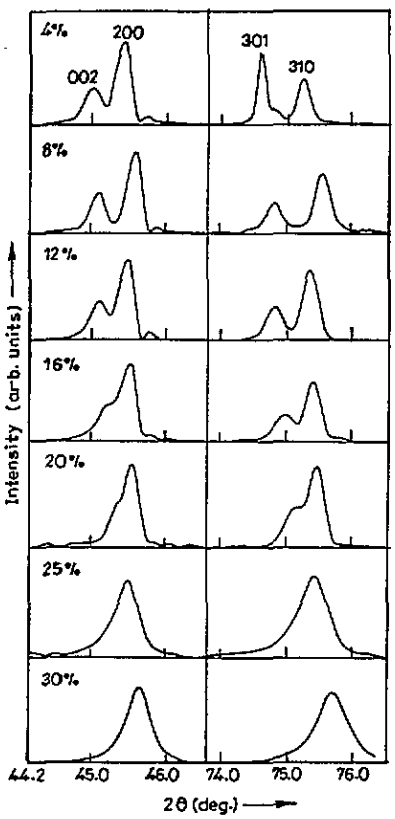

Figure 2. X-ray diffraction profiles of $Ba_{1-x}Sr_xTiO_3$ powders for $x = 0.04$, 0.08, 0.12, 0.16, 0.20, 0.25 and 0.30 for (002)/(200) and (301)/(310) reflections.

Table 1. Lattice parameter and unit-cell volume of $Ba_{1-x}Sr_xCO_3$ for $x = 0.04$, 0.08, 0.12, 0.16, 0.20 and 0.30.

x	a (Å)	b (Å)	c (Å)	V (Å^3)
0.04	5.314	8.909	6.436	304.695
0.08	5.298	8.88	6.414	301.754
0.12	5.288	8.846	6.402	299.47
0.16	5.280	8.832	6.392	298.077
0.20	5.204	9.003	6.382	299.006
0.30	5.151	8.960	6.316	291.502

coprecipitation, unit-cell-level uniform distribution of Sr and Ba ions in each particle, irrespective of its size, is also ensured.

An interesting feature of the variation of the unit-cell parameter with x is that, for the composition range $0.20 \leqslant x \leqslant 0.30$, $b \simeq a\sqrt{3}$ accidentally. This is expected for an orthohexagonal unit cell. As a result, several sets of reflections, such as (200)/(112)/(130), (221)/(041) and (202)/(132), merged into a singlet on the diffractogram in this composition range. Although not given in figure 1, for $x > 0.4$ the situation again departs from $b = a\sqrt{3}$ condition.

2.2. Synthesis and characterization of $(Ba_{1-x}Sr_x)TiO_3$ powders by semi-wet route

In the SW route, $Ba_{1-x}Sr_xCO_3$ powders were mixed with TiO_2 (purity 99%) in stoichiometric proportion in a centrifugal ball mill with agate jar and balls for 4 h. Acetone was used as mixing medium. Mixtures of $Ba_{1-x}Sr_xCO_3$ and TiO_2 for $x = 0.04$, 0.08, 0.12, 0.16, 0.20, 0.25 and 0.30 were calcined at 1150 °C for 12 h and again for 6 h with an intermediate crushing and grinding.

The $Ba_{1-x}Sr_xTiO_3$ system is isomorphous [21] with complete solubility over the entire composition range. $Ba_{1-x}Sr_xTiO_3$ has tetragonal structure at room temperature for a limited range of x. With increasing value of x, tetragonality decreases and the structure becomes cubic at room temperature. There is, however, some controversy about the composition up to which the structure remains tetragonal at room temperature. Drust *et al* [22] and McQuarrie [23] observed cubic phase for $x \geqslant 0.30$. Rushman and Striven [24] have reported tetragonal structure for x up to 0.35 at room temperature. Barb *et al* [4], on the other hand, have reported coexistence of cubic and tetragonal phases even for $x = 0.24$ at room temperature. The volume fraction of the tetragonal phase was reported to decrease for $x > 0.24$, becoming almost cubic for $x = 0.285$.

We find that both the c/a ratio and unit-cell volume first increase up to $x = 0.08$ and then decrease monotonically, with increasing x. This can be inferred from figure 2, which depicts the tetragonal splittings for (002)/(200) and (301)/(310) pairs of reflections. The extent of tetragonal splitting increases up to $x = 0.08$ but then starts decreasing with increasing strontium concentration. For $x = 0.30$, the structure is clearly cubic. It is clear from our observations that the structure becomes cubic at some composition in the range $0.25 < x \leqslant 0.30$, raising doubts about the reports [24] of structure becoming cubic for $x > 0.30$.

2.3. Comparison of compositional homogeneity of powders prepared by dry and semi-wet routes

Some 8% strontium-substituted samples were prepared by the semi-wet route as well as the conventional dry route under identical calcination conditions mentioned in the previous section. For the conventional dry route, $BaCO_3$ (99.5% purity), $SrCO_3$ (99% purity) and TiO_2 (99% purity) were ball milled in stoichiometric proportions for identical duration.

Figures 3(*a*) and (*b*) show diffractometer records for $Ba_{0.92}Sr_{0.8}TiO_3$ powders prepared by the semi-wet and dry routes respectively. Although both the patterns correspond to single-phase specimens, the line splittings characteristic of the tetragonal phase are clearly seen only in figure 3(*a*) for the SW sample. For the dry-route sample, these splittings are barely visible, giving the impression that the structure is pseudo-cubic. Obviously, the tetragonal splittings are masked by compositional inhomogeneities due to microscopic segregation of Ba/Sr ions in the dry-route sample. We have therefore concentrated on samples prepared by the SW route only for the dielectric studies.

The compositional homogeneity of the SW sample was further checked by line broadening analysis of the powder x-ray diffraction profiles. Compositional inhomogeneities in powder specimens lead to fluctuations in d spacings. As a result of this, the diffraction profile will be broadened and its half-width (β) will be given by

$$\beta(\theta) = (\Delta d/d)\tan\theta \tag{1}$$

where θ is the Bragg angle. In addition, there may be broadening caused by the smallness of the particle size. In this case, the half-width is given by the well known Scherrer equation:

$$\beta(\theta) = \lambda/(\bar{D}\cos\theta) \tag{2}$$

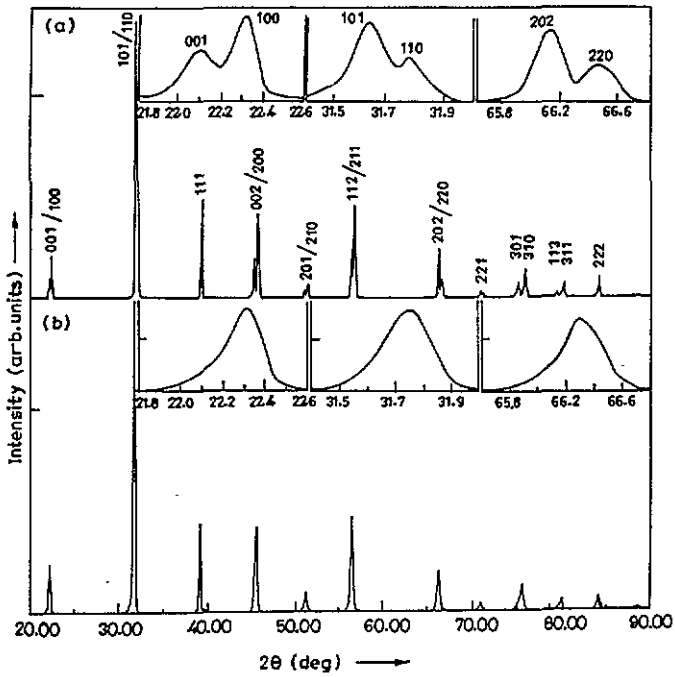

Figure 3. Powder diffractometer records of $Ba_{0.92}Sr_{0.08}TiO_3$ powders prepared by (*a*) semi-wet and (*b*) dry routes.

where λ is the wavelength and $\bar{D}$ is the coherently scattering domain size. Thus in a plot of $\beta\cos\theta$ versus $\sin\theta$, the slope of the straight line will give the level of compositional inhomogeneities whereas the intercept on $\beta\cos\theta$ will give the coherently scattering domain size. In the absence of compositional inhomogeneities, this line should be horizontal.

Prior to performing the line broadening analysis on our samples, the $K\alpha_2$ contribution to the XRD profiles was removed using Rachinger's method. Corrections for the instrumental broadening for various profiles were applied using the half-widths of a standard silicon powder sample. Let B and b be the half-widths of measured profile and silicon standard sample respectively. The half-width of the true diffraction profile will be given by

$$\beta(\theta) = (B^2 - b^2)^{1/2} \tag{3}$$

or

$$\beta(\theta) = B - b \tag{4}$$

depending on whether the true profile is purely Gaussian or Cauchy type. Since real x-ray profiles are never pure Gaussian or Cauchy type, we have used the following empirical relationship, first suggested by Anantharaman and Christian [25], which gives better results:

$$\beta(\theta) = [B - (b^2/B)] \tag{5}$$

Figure 4 gives the $\beta\cos\theta$ versus $\sin\theta$ plots for the semi-wet sample along with the best-fit straight line obtained by least-squares fitting. It is evident from this figure that the straight-line has nearly zero slope, which confirms that the samples prepared by the semi-wet route possess good compositional homogeneity.

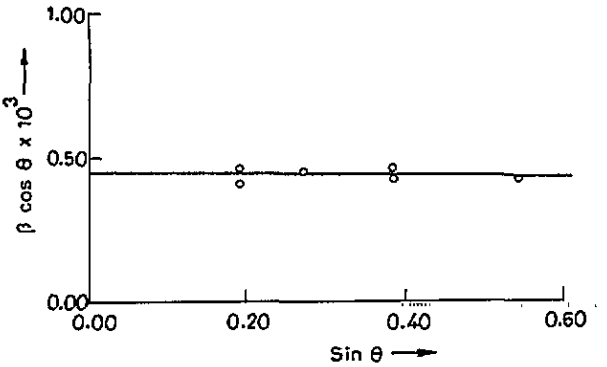

Figure 4. Variation of $\beta \cos\theta$ versus $\sin\theta$ for $Ba_{0.92}Sr_{0.08}TiO_3$ ceramics prepared by the semi-wet route.

3. Dielectric behaviour of $(Ba_{1-x}Sr_x)TiO_3$ ceramics

$Ba_{1-x}Sr_xTiO_3$ powders prepared at 1150 °C by the SW route were compacted in cylindrical dies of 15 mm diameter at a load of 50 kN. Green pellets prepared using powders synthesized at 1150 °C were sintered at 1300 °C for 12 h. The density of the sintered pellets was measured using the liquid displacement method. The sintered density was generally around 95% of the theoretical density for different compositions.

For dielectric measurements, sintered pellets of $Ba_{1-x}Sr_xTiO_3$ ceramics were electroded with air dry silver paste on polished surfaces that were pretreated with isopropanol in order to remove the adsorbed water molecules from the surface [26]. All dielectric measurements were carried out using an HP 4192A LF Impedance Analyser. Temperature was controlled within ±1 °C during dielectric measurements.

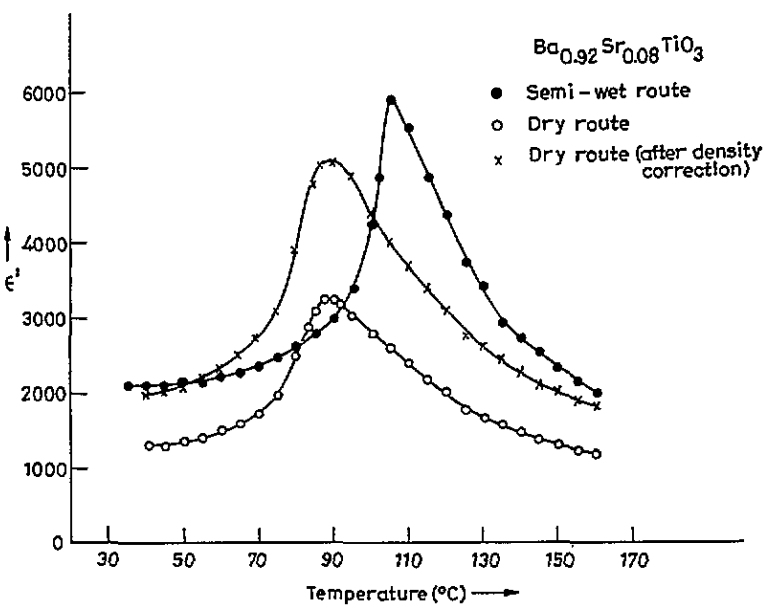

Figure 5. Temperature dependence of ϵ' at 100 kHz for $Ba_{0.92}Sr_{0.08}TiO_3$ ceramics fabricated by semi-wet and conventional dry routes.

3.1. Effect of synthesis route on the dielectric behaviour

Figure 5 depicts the temperature dependence of ϵ' measured at 100 kHz for $Ba_{0.92}Sr_{0.08}TiO_3$ ceramics prepared by SW and conventional D routes. Since the ϵ' values are dependent on the density of the specimen (which was 95 and 90% of the theoretical density for SW and D routes respectively), we have applied corrections to the ϵ' values of conventionally prepared samples so that both correspond to equivalent densities using the relationship given in [27]. It is evident from figure 5 that the ϵ' versus T curve is smeared out in both cases although it is a little more so in the conventionally prepared sample. The difference in T'_m for the two samples could be due to the presence of impurities like Fe, which can reduce T'_m drastically even if they are present in traces. The fact that the smearing of the ϵ' versus T curve persists even in SW route samples with good compositional homogeneity indicates that the compositional inhomogeneities can enhance the smearing but may not be primarily responsible for it.

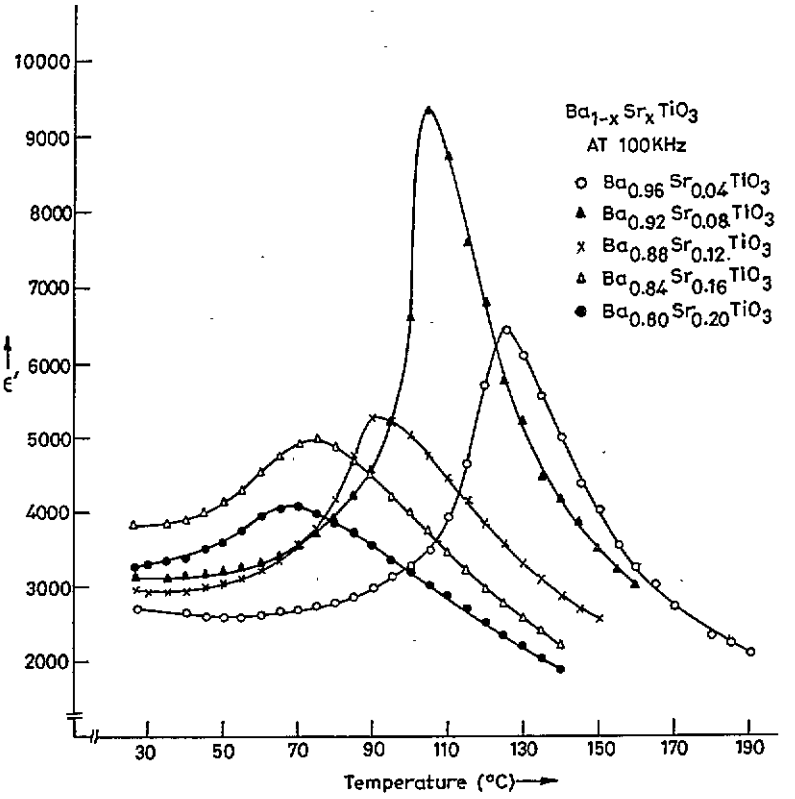

Figure 6. Temperature dependence of ϵ' for $Ba_{1-x}Sr_xTiO_3$ ceramics fabricated by semi-wet route, measured at 100 kHz for $x = 0.04$, 0.08, 0.12, 0.16 and 0.20.

3.2. Effect of Sr content on the dielectric behaviour

Figure 6 depicts the effect of strontium content on the temperature dependence of dielectric constant measured at 100 kHz for the compositionally homogeneous $Ba_{1-x}Sr_xTiO_3$ ceramics

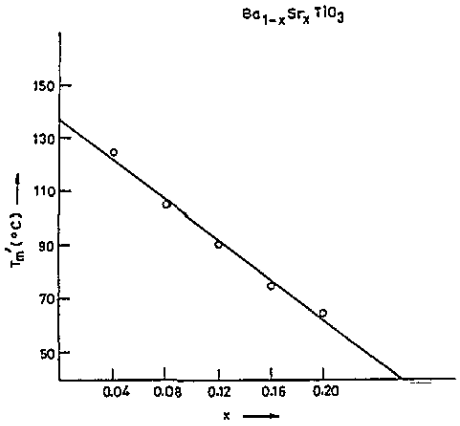

Figure 7. Variation of T_m' with strontium content (x) for $Ba_{1-x}Sr_xTiO_3$ ceramics fabricated by semi-wet route.

prepared by the SW route for $x = 0.04$, 0.08, 0.12, 0.16 and 0.20. Figure 7 shows the variation of T_m' (i.e. the temperature at which ϵ' is maximum) with strontium concentration (x). It is evident from this figure that T_m' decreases linearly with strontium content (x) in agreement with similar observations on dry-route samples by earlier workers [3, 28]. A least-squares fit of straight line to the data points to figure 7 gives the rate of decrease of T_m' with strontium content as 3.75 °C/mol.% of $SrTiO_3$, in excellent agreement with that reported by Jackson and Reddish [28] and Jaffe *et al* [3], even though the absolute values of T_m' in our case were always higher than those reported by earlier workers.

The peak value of dielectric constant ϵ_m' of $Ba_{1-x}Sr_xTiO_3$ at T_m' increases with x up to $x = 0.08$ and then exhibits a monotonic decrease for $x > 0.08$ as can be seen from figure 6. This is consistent with our x-ray observations also according to which tetragonality first increases up to $x = 0.08$ and thereafter starts decreasing (see figure 2). Further, the smearing of the ϵ' versus T curve increases with increasing Sr content. This further supports our contention that the smeared response in $Ba_{1-x}Sr_xTiO_3$ samples prepared by SW route is intrinsic to the system and is caused by the partial substitution of Ba^{2+} by Sr^{2+}.

3.3. Departure from Curie–Weiss behaviour and relevant critical exponents

Even in pure $BaTiO_3$ crystals, departure from the Curie–Weiss law has been reported up to 5 K above T_c [29]. In $Ba_{1-x}Sr_xTiO_3$, the departure from Curie–Weiss behaviour is observed over a much wider temperature range. Figure 8 depicts the variation of dielectric stiffness ($1/\epsilon'$) with temperature for different Sr content. It is evident that the departure from Curie–Weiss behaviour increases with increasing Sr content. Since the smearing also increases with increasing Sr content, the two should be interlinked. A similar behaviour was recently reported by us for $Ba_{1-x}Ca_xTiO_3$ [14].

The temperature dependence of dielectric stiffness for $BaTiO_3$, which undergoes a weakly first-order phase transition around 130 °C, can be written as

$$1/\epsilon' = 1/\epsilon_m' + (T - T_m')/C' \tag{6}$$

where ϵ_m' is the discontinuous jump in ϵ' at the thermodynamic phase transition temperature T_m' [30] and C' is a Curie–Weiss-like constant. The above relationship follows from the fact that in a first-order phase transition there is no singularity in ϵ' at the thermodynamic phase transition temperature, which is invariably higher than the critical temperature T_c for the corresponding second-order phase transition [30]. For dirty displacive ferroelectrics, the dielectric stiffness exhibits [14, 18] a slightly modified temperature dependence:

$$1/\epsilon' = 1/\epsilon_m' + (T - T_m')^\gamma/C' \tag{7}$$

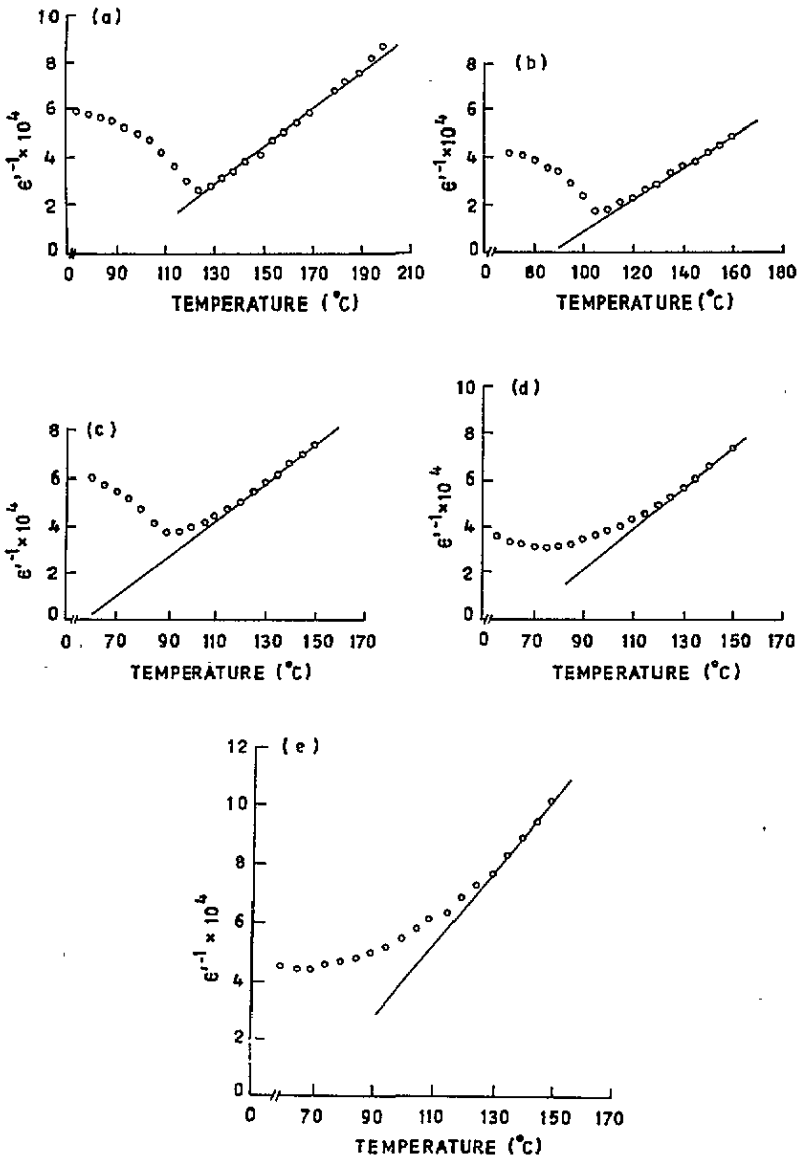

Figure 8. Temperature dependence of dielectric stiffness ($1/\epsilon'$) of $Ba_{1-x}Sr_xTiO_3$ ceramics for $x = 0.04$ (*a*), 0.08 (*b*), 0.12 (*c*), 0.16 (*d*) and 0.20 (*e*).

where $\gamma \simeq 1$ for NDF whereas $1 < \gamma \leqslant 2$ for DDF.

We have determined the critical exponent γ for samples with $x = 0.04$, 0.08, 0.12, 0.16 and 0.20 in the manner adopted for $Ba_{1-x}Ca_xTiO_3$ ceramics [14]. Figure 9 shows the $\ln(1/\epsilon' - 1/\epsilon'_m)$ versus $\ln(T - T'_m)$ plots for different values of x. The variations of critical exponent γ and Curie–Weiss-like constant C' with x are shown in figure 10. It is evident from this figure that the critical exponent γ lies between 1.32 and 1.76 for $0.04 \leqslant x \leqslant 0.16$, which is very different from the mean-field exponent ($\gamma = 1$) but is in agreement with similar observations [14, 18] on other dirty displacive ferroelectrics.

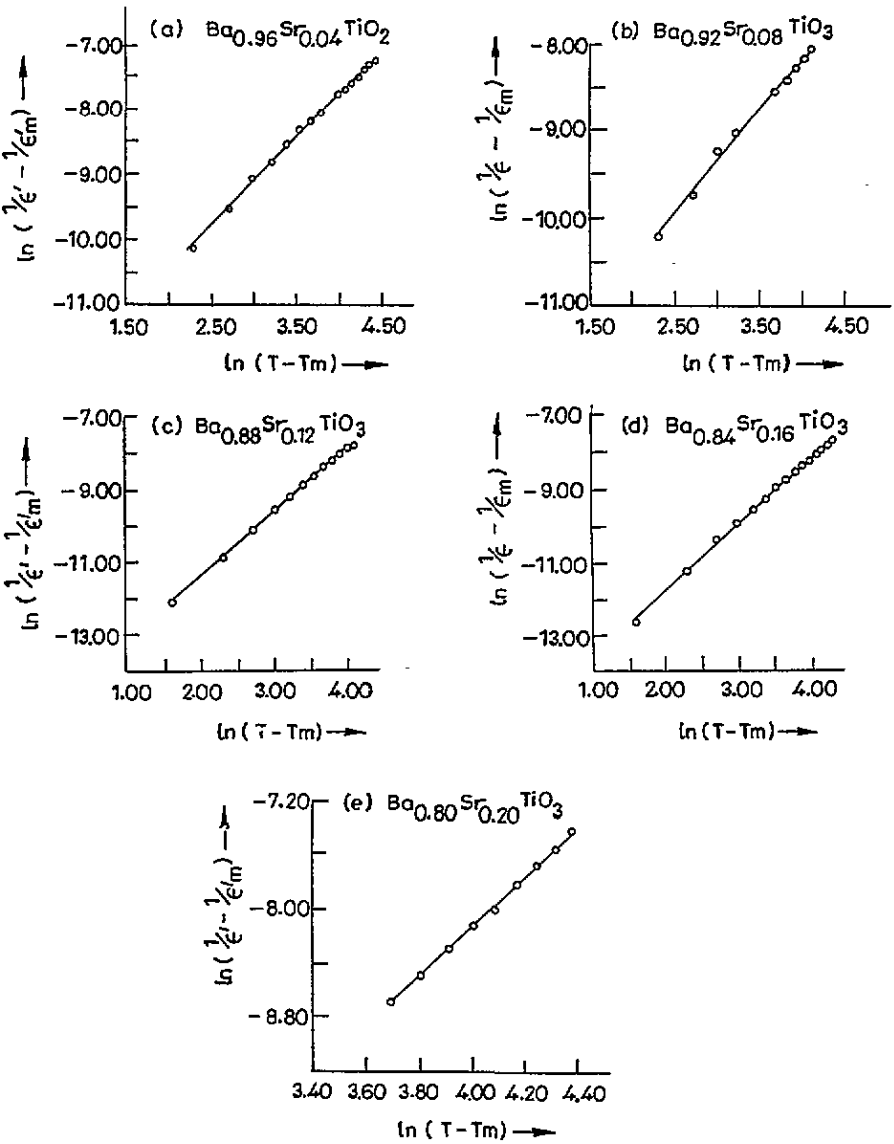

Figure 9. Variation of $\ln(1/\epsilon'_m - 1/\epsilon')$ with $\ln(T - T'_m)$ of $Ba_{1-x}Sr_xTiO_3$ ceramics for $x = 0.04$ (*a*), 0.08 (*b*), 0.12 (*c*), 0.16 (*d*) and 0.20 (*e*).

Further, the Curie–Weiss-like constant C', which is of the order of 2×10^5 K^{-1} for $BaTiO_3$ exhibiting sharp transitions, increases with Sr content. For higher Sr contents, the value of C' rapidly approaches the values reported for other dirty displacive ferroelectrics [14, 18]. It is interesting to note that the extrapolation of the best-fit line for γ versus x plot to $x = 0$ gives $\gamma = 1.10$, which is in good agreement with $\gamma = 1.08$ reported by Uchino and Namura [18] for $BaTiO_3$ single crystals. It may be further noted that, with increasing Sr content, the exponent γ will approach 2, which is expected for quantum ferroelectrics [31]. The ferroelectric state seems to get destabilized with increasing Sr^{2+} content.

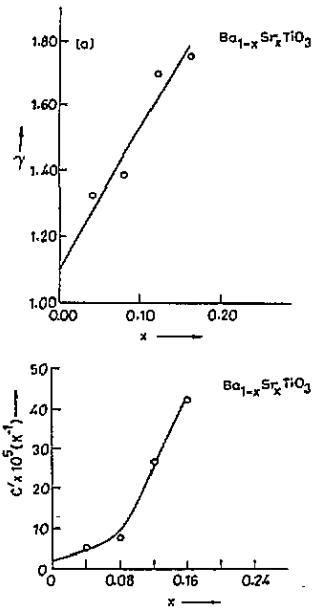

Figure 10. Variation of (*a*) critical exponent (γ) and (*b*) Curie–Weiss-like constant (C') with strontium content (x) for $Ba_{1-x}Sr_xTiO_3$ ceramics.

3.4. Relaxational dipolar freezing and dipole glass behaviour

Near the normal ferroelectric phase transition temperature, the susceptibility χ, relaxation time τ and correlation length ξ all diverge, with exponents related to scaling laws, i.e. $\chi \sim (T - T_c)^{-1}$, $\tau \sim (T - T_c)^{-\delta}$, and $\xi \sim (T - T_c)^{-\nu}$ where T_c is the critical temperature [19]. In the case of smeared transitions, we have seen in the previous section that the divergence of χ is less critical at T'_{max} ($1 < \gamma < 2$). This is similar to what is observed in several dipole/orientational glasses [19]. However, the lack of divergence or discontinuous jump in χ and ξ at T_c is necessary but not sufficient for a material to qualify as a glass, since these quantities remain finite even in normal ferroelectrics below the Curie point on account of the domain state, which has its origin in the surface energy contributions and finite size effect. For a non- or less-critical response leading to dipole glass, there should be a characteristic dynamic (frequency-dependent) response below T'_{max} in support of gradual relaxational freezing as against 'critical slowing down' at T_c in systems undergoing normal ferroelectric phase transition. In this section, we present experimental evidence for relaxational freezing in (Ba,Sr)TiO$_3$.

To understand the nature of dielectric relaxation, we first scanned ϵ' and ϵ'' at various frequencies below 1 MHz at room temperature for $Ba_{1-x}Sr_xTiO_3$ with $x = 0.08$, 0.12, 0.16 and 0.20. These are plotted in figure 11. It is evident from this figure that the peak in ϵ'' occurs near the inflection point for ϵ' versus frequency curve. This suggests Debye-like relaxation behaviour. It may be noted that, with increasing Sr content, the location of ϵ'' peak shifts to the lower-frequency side, which implies that the relaxation time τ increases wtih increasing Sr content. The real (ϵ') and imaginary (ϵ'') parts of the dielectric constant for Debye-type relaxation are known to follow the relationship

$$\epsilon' = \epsilon_\infty - \tau\omega\epsilon'' \tag{8}$$

where ϵ_∞ is the high-frequency dielectric constant while ω is 2π times the measuring frequency. Figure 12 depicts the ϵ' versus $\omega\epsilon''$ plots along with the least-squares straight-line fits for $x = 0.08$, 0.12, 0.16 and 0.20 at room temperature. Excellent straight-line fits

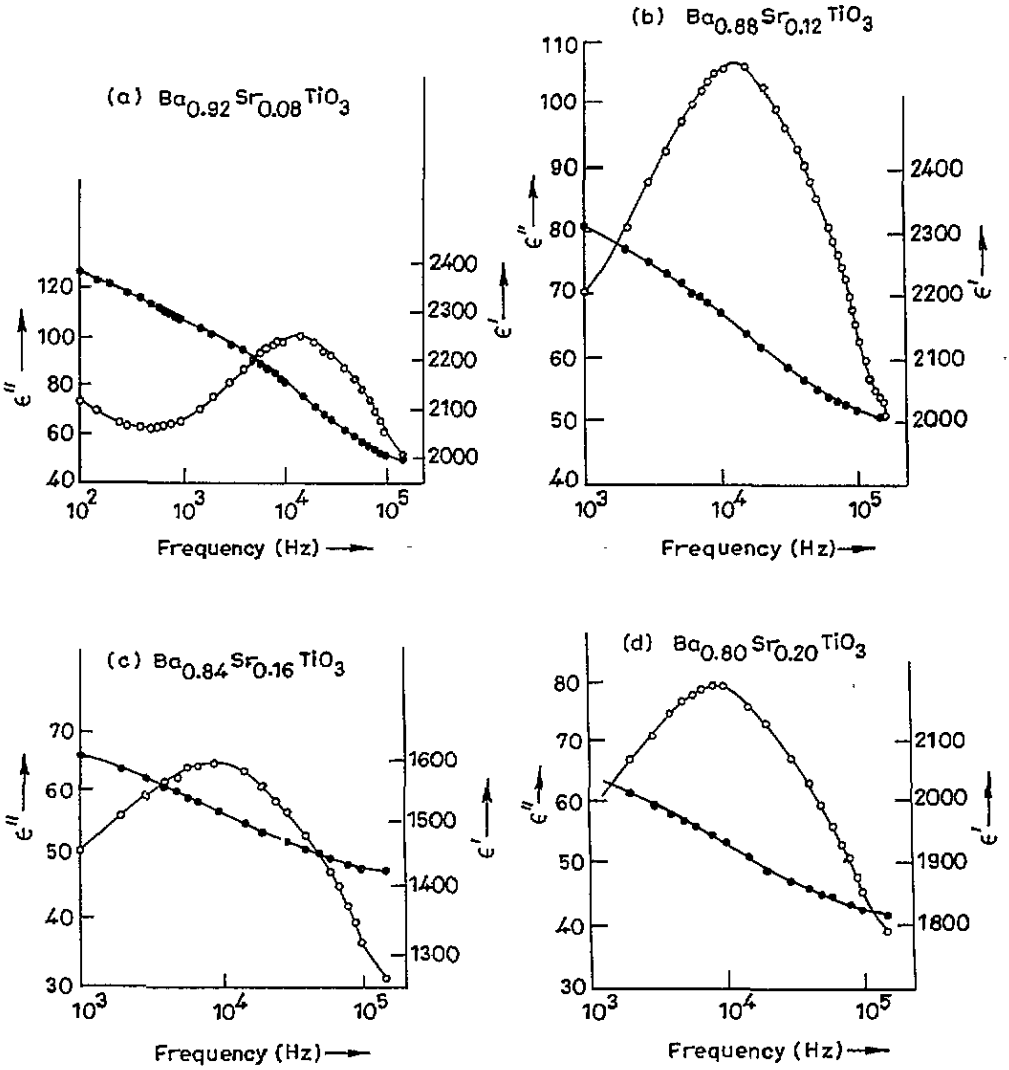

Figure 11. Frequency dependence of ϵ' and ϵ'' for $Ba_{1-x}Sr_xTiO_3$ ceramics for (*a*) $x = 0.08$, (*b*) $x = 0.12$, (*c*) $x = 0.16$ and (*d*) $x = 0.20$ at room temperature.

further confirm Debye-like relaxation. Table 2 lists the relaxation time obtained from these fits for different Sr contents.

In order to study the temperature dependence of relaxation time, we measured ϵ' and ϵ'' at frequencies ranging from 100 Hz to 500 kHz at various temperatures below T_m' for 8% strontium. The results are shown in figure 13. It is evident from this figure that the position of the Debye loss peak due to relaxational dispersion shifts to higher frequencies with increasing temperature similar to what is known for relaxational systems such as dipole glasses [19]. The situation above T'_{max} was not very clear due to sudden rise of ϵ'' beyond 100 kHz presumably due to increased conductivity losses at higher temperatures. Since the position of the loss peak is determined by the condition $\omega\tau = 1$, it follows that the relaxation time of the dielectric polarization process decreases with increasing temperature

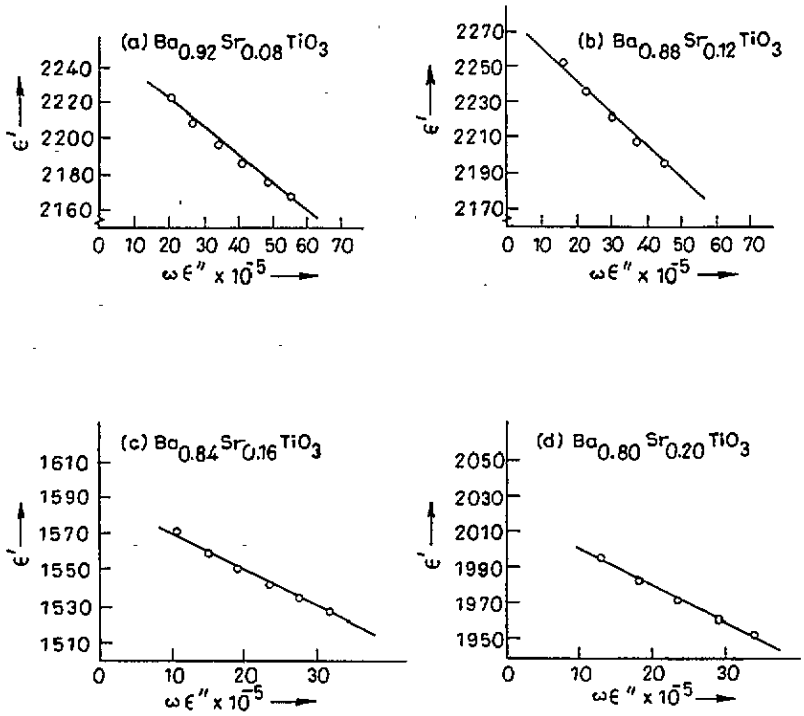

Figure 12. Straight-line fits between ϵ' and $\omega\epsilon''$ of $Ba_{1-x}Sr_xTiO_3$ ceramics for (*a*) $x = 0.08$, (*b*) $x = 0.12$, (*c*) $x = 0.16$ and (*d*) $x = 0.20$.

Table 2. Variation of relaxation time (τ) with Sr content for $Ba_{1-x}Sr_xTiO_3$ ceramics.

x	Relaxation time (10^{-7} s)
0.08	156.2
0.12	182.1
0.16	197.0
0.20	206.0

up to T'_{max}.

The relaxation time (τ) at various temperatures calculated using equation (1) from the slope of the straight lines fitted to the ϵ' and $\omega\epsilon''$ values in the least-squares sense are listed in table 3. It is evident from this table that the relaxation time (τ) decreases with increasing temperature. Similar decrease of τ with increasing temperature has been reported for relaxor ferroelectrics such as lead lanthanum zirconate titnate (PLZT) [32], strontium barium niobate (SBN) [32,33] and lead indium niobate (PIN) [34]. In these systems, an Arrhenius-type temperature dependence for τ has been verified

$$\tau = \tau_0 \exp(\Delta E/kT) \tag{9}$$

where ΔE is the activation energy, k is the Boltzmann constant, T is absolute temperature and τ_0 is the inverse of attempt frequency. A plot of $\ln\tau$ as a function of T^{-1} is given in figure 14. The activation energy ($\Delta E/k$) and τ_0 calculated from least-squares fit to the data points, are 4993 K and 1.136×10^{-12} s, respectively. The activation energy obtained

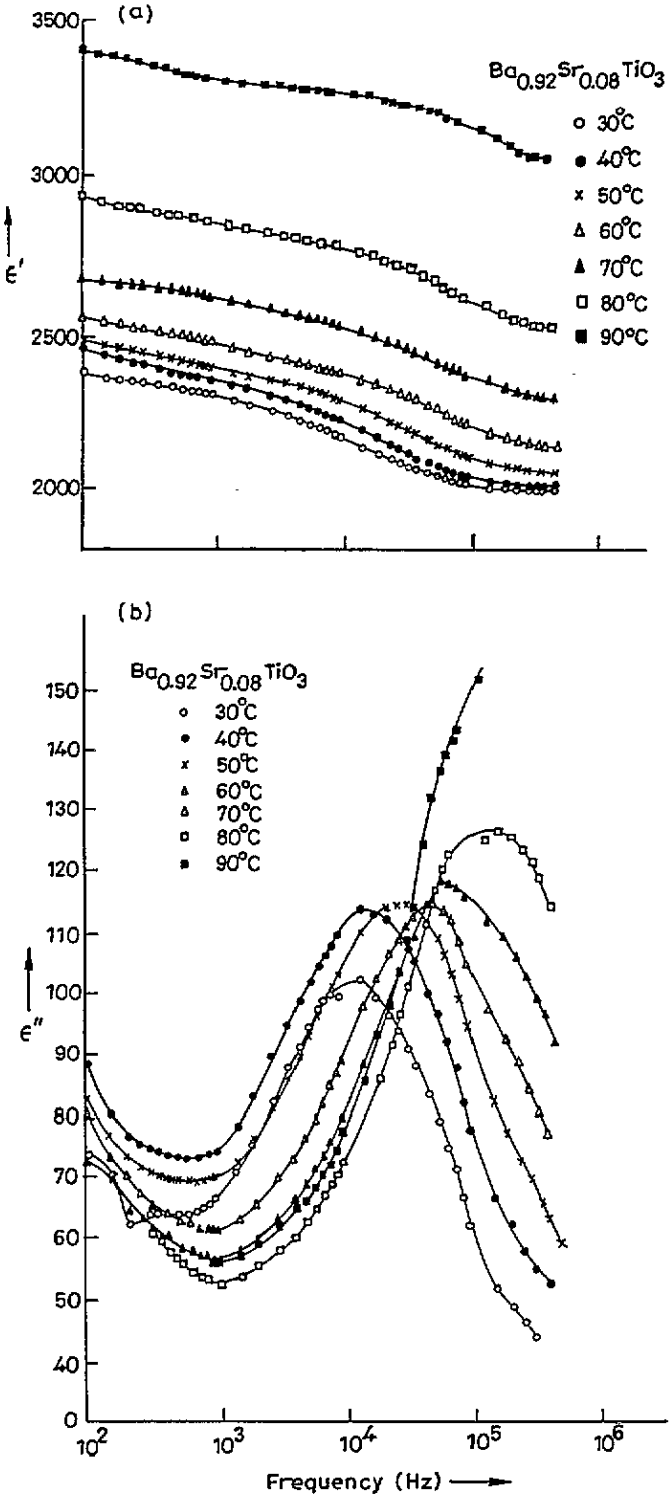

Figure 13. Frequency dependence of (*a*) ϵ' and (*b*) ϵ'' for $Ba_{0.92}Sr_{0.08}TiO_3$ ceramic at different temperatures.

Table 3. Temperature dependence of relaxation time (τ) for $Ba_{0.92}Sr_{0.08}TiO_3$ ceramics below the hump temperature.

T (°C)	Relaxation time (10^{-7} s)
30	156.2
40	133.5
60	37.9
70	31.6
80	21.7
90	9.3

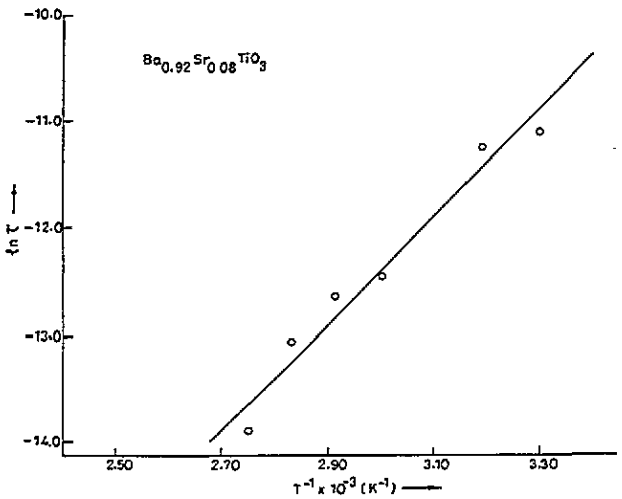

Figure 14. Arrhenius-type temperature dependence of relaxation time (τ) for $Ba_{0.92}Sr_{0.08}TiO_3$ ceramics.

in this system is in good agreement with the activation energies reported for PLZT [32], SBN [32, 33] and PIN [34].

The Debye-like dielectric relaxation in (Ba,Sr)TiO_3 with relaxation times in the range of 10^{-5} and 10^{-7} s cannot be attributed to the elementary dipoles, which are expected to relax at much higher frequencies in the microwave to infrared regions. The large relaxation times indicate that the Debye-type relaxation is associated with the relaxation of a cluster of dipoles. The relaxation time of the order of 10^{-6} s has been observed [29] even in pure $BaTiO_3$ above T_c just before the polar clusters freeze abruptly near T_c. At temperatures well above T_c or below T_c, τ lies between 10^{-9} and 10^{-10} s [35]. The low value of τ in the critical regions for $BaTiO_3$ has been attributed to the dynamics of polar clusters after the cross-over [36] from displacive to order–disorder limits. These polar clusters in pure $BaTiO_3$ freeze [35] over a very narrow temperature range of a fraction of a degree celsius as expected for a normal phase transition. In the case of $Ba_{1-x}Sr_xTiO_3$, the relaxation time gradually increases with decreasing temperature below T'_m. This is akin to relaxational freezing (in contrast to static freezing or critical slowing down in $BaTiO_3$) observed in dipole glasses [19]. The relaxation time follows Arrhenius-type behaviour observed in several glassy systems and the hump temperature T'_m should therefore be the freezing temperature in analogy to the behaviour reported for dipole glasses [19].

The freezing temperature T'_m in glassy systems is generally known to depend on the frequency of the applied field [19] although there are some exceptions in the spin-glass systems [37]. Figure 15 depicts the effect of varying frequency on the temperature dependence of ϵ' and ϵ'' for $x = 0.20$. The origins of the curves in this figure have been

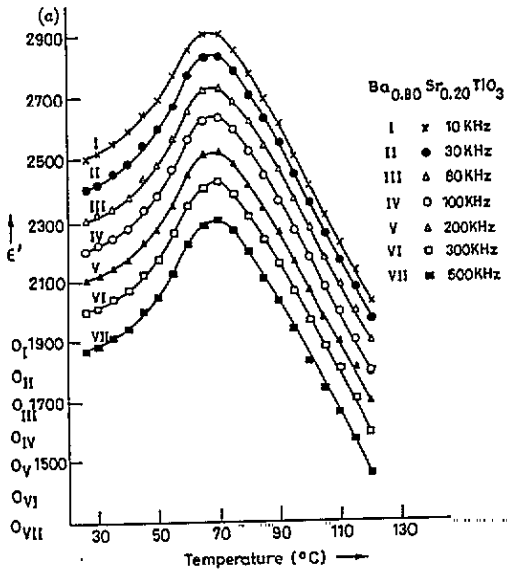

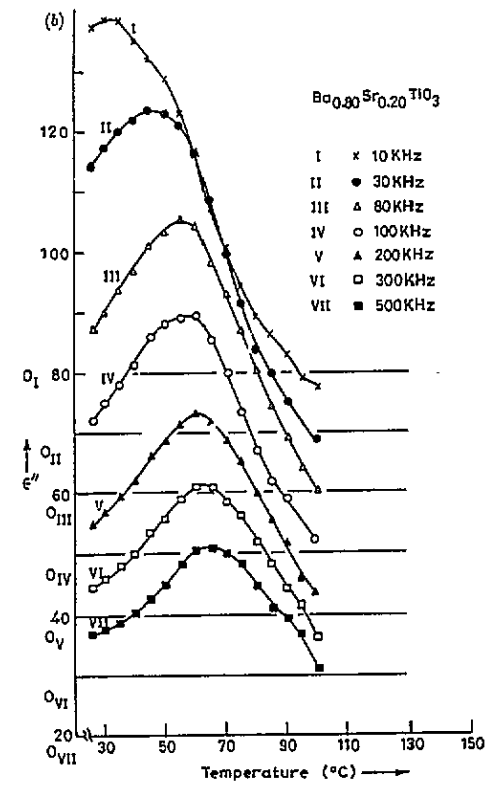

Figure 15. Temperature dependence of ϵ' and ϵ'' at various frequencies for $Ba_{0.80}Sr_{0.20}TiO_3$ ceramics. Origin for each curve is shifted vertically along y axis to avoid overlapping of curves at different frequencies.

shifted vertically for the sake of clarity. It is evident from this figure that both T'_m and T''_m shift to higher temperatures with increasing frequency, although the shift is more pronounced for T''_m than for T'_m. It is worth mentioning that, with decreasing Sr content, the magnitude of these shifts decreases, indicating the role of quenched random disorder due to strontium substitution in frustrating the development of ferroelectric order. The observation of these shifts lends further support to our contention that T'_{max} is not a regular phase transition temperature but is akin to freezing temperature observed in glassy systems.

4. Concluding remarks

From the experimental evidence presented in the foregoing sections, it can be inferred that the smeared or diffuse transition in (Ba,Sr)TiO_3 ceramics is intrinsic to the system and does not seem to be due to extrinsic factors such as compositional inhomogeneities. Marked departures from the Curie–Weiss law above T'_{max} are observed as a result of strontium substitution; the temperature range for this departure is found to increase with increasing strontium content. This is similar to what is reported for PLZT [38] and (Ba,Ca)TiO_3 [14] with diffuse transition and $(K_{1-x}Na_x)NbO_3$ [19] with orientational glass transition. In all these systems, including the present one, the exponent γ for the scaling relationship for ϵ' versus T is found to increase gradually from the mean-field value ($\gamma = 1$) towards $\gamma = 2$ with increasing concentration of substituting cation. Even in pure $BaTiO_3$ crystals, departure from Curie–Weiss behaviour has been reported [29, 39] up to 5 K above the transition temperature. Over this temperature range, the presence of polar clusters has also been observed [29, 39] as fluctuations. More recently, it has been reported [40] that the polar phase persists over the entire temperature range (35 °C) of departure from the Curie–Weiss law in (Ba,Ca)TiO_3, which also exhibits diffuse transition. A similar situation has recently been observed in the (Ba,Sr)TiO_3 system with 8% strontium [41].

In $BaTiO_3$, the presence of polar clusters above the phase transition temperature is believed [42] to be linked with the cross-over from the displacive to the order–disorder limit. Experimental support for this picture comes from the observation of: (i) a strong polar relaxation mode in the frequency range 10^8–10^9 [43], and (ii) the off-centre displacement of Ti^{4+} ions by electron paramagnetic resonance (EPR) studies [36, 44] in the cubic phase. The correlation volume for the polar clusters above the phase transition temperature has been estimated [43] to be 4000 Å^3. We feel that in the strontium-substituted samples also, the system prepared for a regular phase transition as in any typical displacive system at high temperatures but soon crossed over to the coupled soft mode relaxation regime as the temperature is lowered. This was followed by a gradual relaxational freezing of the polar cluster dynamics over a barrier height of about 4993 K, instead of the 'critical slowing down' of the relaxation process expected for a regular ferroelectric phase transition as in pure $BaTiO_3$. The shifts in (i) the Debye loss peaks as a function of temperature and (ii) the T'_{max} and T''_{max} as a function of frequency provide experimental evidence in support of the formation of orientational/dipole glass state. It is interesting to note that the room-temperature tetragonal structure cannot be taken as a signature of a ferroelectric phase transition with true long-range order. In fact, the size of the dipolar clusters undergoing relaxational freezing below T'_m is big enough to exhibit the 'local symmetry breaking' on XRD patterns but is smaller than the critical size required to stabilize the true long-range ferroelectric order against thermal fluctuations. Nevertheless, even a very small external electric field can induce ordering and freezing of these dipolar clusters at suitably low temperatures reminiscent of high responsiveness of superparamagnetic clusters.

Historically, Burns and coworkers [9, 45] were the first to propose that the mixed/complex oxide ferroelectrics with diffuse transitions exhibit glassy polarization behaviour. Their suggestion was mainly based on the marked departure of index of refraction $n(T)$ from linear temperature dependence up to a characteriztic temperature T_d well above T'_m in several dirty displacive ferroelectrics. We have also noted marked departures of dielectric stiffness $(1/\epsilon')$ from Curie–Weiss behaviour with Sr content over a wide temperature range above T'_m. It was shown by Burns and coworkers that between T_d and T'_m the $n(T)$ data can be rationalized in terms of local, randomly oriented polarization with dynamic origin. According to these workers, the random polar regions present above T'_m undergo normal ferroelectric transition below T'_m. Thus, in their model, the system is in a glassy polarization phase between T_d and T'_m only and undergoes a normal ordering transition below T'_m. No attempt was made by these workers to verify if the polar regions present above T'_m undergo relaxational freezing as expected for a truly glassy phase even though these workers had noted glass-like features in low-temperature ($T < T'_m$) specific heat. Through dielectric spectroscopic studies at $T < T'_m$, we have clearly shown that, in the $Ba_{1-x}Sr_xTiO_3$ system, the polar regions supposedly present above T'_m undergo a relaxational freezing below T'_m. It will be interesting to study the dielectric behaviour of field cooled samples and look for the divergence in the second- and higher-order non-linear coefficients of susceptibility as has been recently shown [46] for the $Pb(Mg_{1/3}Nb_{2/3})O_3$ system exhibiting diffuse transition and dipole glass behaviour.

Before we end, we would like to mention that the relaxational dipolar freezing observed in (Ba,Sr)TiO_3 (BST) has features that are different from those reported for $Pb(Mg_{1/3}Nb_{2/3})O_3$ (PMN) even though both systems exhibit smeared transitions. First of all, the frequency dispersion of T'_m in PMN is quite large (> 20 °C) as compared to BST where it is less than 5 °C for $x \geqslant 0.16$. The large frequency dispersion of T'_m in PMN has been analysed [46] in terms of Vogel–Fulcher (VF) relationship $\tau = \tau_0 \exp[\Delta E/k(T'_m - T_f)]$ with T_f being the VF freezing temperature, which for PMN has been found to be about 50 °C lower than T'_m [47]. Earlier attempts to fit an Arrhenius-type relationship gave [15] very unrealistic values for ΔE (1.5 and 7 eV in high- and low-temperature regions) and τ_0 (10^{-38} s). In the case of BST, it is not possible to prove or disprove the applicability of VF freezing because of the poor resolution of temperature measurement (±1 °C) and very small frequency dispersion of T'_m. In PMN it has been found that the dielectric dispersion becomes markedly non-Debye-type with very wide distribution of relaxation times near T_f [47]. In BST (8%) the dielectric dispersion remains essentially Debye-type right up to room temperature, which is more than 70 °C lower than T'_m. There is, however, some evidence for the cessation of the temperature-dependent relaxation process since the position of the loss peak below 40 °C does not change (see figure 13(*b*)). This implies freezing of the cluster dynamics around 40 °C, but a higher-resolution experiment is needed to establish if this temperature is similar to the T_f of VF relationship. We must add that, like BST, there are other glassy systems like $K(Ta,Nb)O_3$ [48] and $(K,Na)TaO_3$ [49] where relaxation remains essentially Debye-like and the relaxation time shows Arrhenius-type temperature dependence. The difference in the dielectric relaxation behaviours of BST and PMN may be due to the difference in the chemistry of these systems. While the BST samples are compositionally homogeneous, PMN is known to contain nanometre-scale heterogeneities in terms of the presence of ordered and disordered regions [50]. Further, the ordered and disordered regions have excess negative and positive charges owing to the difference in their chemical compositions, i.e. $Pb(Mg_{1/2}Nb_{1/2})O_3$ and $Pb(Mg_{1/4}Nb_{3/4})O_3$ [50]. The giant dipole moments associated with these ordered and disordered regions have nothing to do with any structural phase transition and are decoupled at high temperatures. On cooling, the

local field couples these moments at $T_f < T < T_m'$ until at T_f the polarization fluctuations undergo Vogel–Fulcher freezing into a dipole glass state [51]. In contrast, the diffuse transition in BST is intimately linked with the ferroelectric transition in $BaTiO_3$. Since the ionic radius of Sr is slightly lower than that of Ba, it is likely to occupy slightly off-centre positions along ⟨100⟩ axes with respect to unit-cell corner sites occupied by Ba in a manner analogous to Li and Na occupancies in (K,Li)TaO_3 and (K,Na)TaO_3 [19]. Such an off-centre occupancy of Sr may generate random local fields conjugate to the order parameter and thereby influence the critical behaviour of the system [52, 53]. As shown by Imry and Ma [52], it is energetically favourable for such systems to split into domains whose size will be governed by domain-wall energy and random field (RF). With increasing concentration of the quenched impurities responsible for the random field, the domain size may become comparable to the correlation length for spatial fluctuations of the order parameter and ferroelectric state may eventually give way to a dipolar glass state. The features described in the present work suggest that Sr substitution in small concentration leads to mesoscopic RF domains, which degenerate into frustrated dipolar clusters for higher Sr concentration such as BST 20%, where T_m' exhibits the frequency dispersion characteristic of a dipole glass.

Acknowledgment

This work was partially supported by the Inter University Consortium for the Department of Atomic Energy Facilities of India.

References

[1] Smolenskii G A and Rozgachev K I 1954 *Zh. Tekh. Fiz.* **24** 1751
[2] Smolenskii G A and Isupov V A 1954 *Dokl. Akad. Nauk. SSSR* **96** 53
[3] Jaffe B, Cook W R and Jaffe H 1971 *Piezoelectric Ceramics* (New York: Academic)
[4] Barb D, Barbulescu E and Barbulescu A 1982 *Phys. Status Solidi* a **74** 79
[5] Bethe K and Welz F 1971 *Mater. Res. Bull.* **6** 209
[6] Coufova B, Janousek V and Novak J 1972 *Czech.* B **22** 485
[7] Benguigui L and Bethe K 1976 *J. Appl. Phys.* **47** 2787
[8] Benguigui L 1978 *Phys. Status Solidi* a **46** 337
[9] Burns G 1987 *Phys. Rev.* B **13** 215
[10] Smolenskii G A 1970 *J. Phys. Soc. Japan* **28** 26
[11] Schmidt G 1990 *Phase Trans.* **20** 127
[12] Hennings D, Schnell A and Simon G 1982 *J. Am. Ceram. Soc.* **65** 11
[13] Tiwari V S, Pandey D and Groves P 1989 *J. Phys. D: Appl. Phys.* **22** 837
[14] Tiwari V S and Pandey D 1994 *J. Am. Ceram. Soc.* II **77** 1819
[15] Kirillov V V and Isupov V A 1973 *Ferroelectrics* **5** 3
[16] Setter N 1980 *PhD Thesis* Pennsylvania State University
[17] Cross L E 1987 *Ferroelectrics* **76** 241
[18] Uchino K and Namura S 1982 *Ferroelectric. Lett.* **44** 56
[19] Höchli U T, Knorr K and Löidl A 1990 *Adv. Phys.* **39** 599
[20] Tiwari V S, Singh N and Pandey D 1994 *J. Am. Ceram. Soc.* I **77** 1813
[21] Basmajian A and De Veries R C 1957 *J. Am. Ceram. Soc.* **40** 373
[22] Drust G, Grotenhuis M and Barkow A G 1950 *J. Am. Ceram. Soc.* **33** 133
[23] McQuarrie M 1955 *J. Am. Ceram. Soc.* **38** 444
[24] Rushman D F and Striven M A 1946 *Trans. Faraday Soc.* **42A** 231
[25] Anantharaman T R and Christian J W 1956 *Acta Crystallogr.* **9** 479
[26] Mountvala A J 1971 *J. Am. Ceram. Soc.* **54** 544
[27] Reddish W, Plessner W and Jackson W 1946 *Trans. Faraday Soc.* **42A** 244
[28] Jackson W and Reddish W 1945 *Nature* **156** 717

[29] Zvirgzd J A, Zvirgzd J V and Fritsberg V J 1989 *J. Phys. Soc. Japan* 49 166
[30] Lines M E and Glass A M 1977 *Principles and Applications of Ferroelectrics and Related Materials* (Oxford: Clarendon)
[31] Rytz D, Höchli U T and Bilz H 1980 *Phys. Rev.* B **22** 359
[32] Kersten O, Rost A and Schmidt G 1983 *Phys. Status Solidi* a 75 495
[33] Glass A M 1969 *J. Appl. Phys.* **40** 4699
[34] Groves P 1985 *Ferroelectrics* 65 67
[35] Magliona M and Jannot B 1991 *Phase Trans.* 33 123
[36] Müller K A, Berlingner W and Albers J 1985 *Phys. Rev.* B 32 5837
[37] Tholence J L 1980 *Solid State Commun.* 35 113
[38] Stenger C G F and Burggraf A J 1980 *J. Phys. Chem. Solids* 41 25
[39] Kanzig V W 1951 *Helv. Phys. Acta.* 24 175
[40] Tiwari V S, Pandey D, Krishna P S R, Chakravarthy R and Dasannacharya B A 1991 *Physica* B **174** 112
[41] Singh N, Singh A P and Pandey D to be published
[42] Bruce D A and Cowley R A 1981 *Structural Phase Transition* (London: Taylor & Francis)
[43] Maglione M, Bohmer R, Löidl A and Höchli U T 1989 *Phys. Rev.* B **40** 11 441
[44] Müller K A, Berlinguer W and Albers J 1985 *Phys. Rev.* B 34 6130
[45] Burns G and Dacol F H 1983 *Phys. Rev.* B 28 2527; 1986 *Solid State Commun.* 58 567
[46] Viehland D, Jang S J, Cross L E and Wuttig M 1991 *J. Appl. Phys.* 69 414
[47] Viehland D, Jang S, Cross L E and Wuttig M 1991 *Phil. Mag.* B 64 335
[48] Samara G A 1984 *Phys. Rev. Lett.* 53 298
[49] Maglione M, Höchli U T and Joffrin J 1986 *Phys. Rev. Lett.* 57 436
[50] Boulesteix C, Varnier F, Llebaria A and Husson E 1994 *J. Solid State Chem.* **108** 141
[51] Viehland D, Li J F, Jang S J and Cross L E 1991 *Phys. Rev.* B 43 8316
[52] Imry Y and Ma S 1975 *Phys. Rev. Lett.* 35 1399
[53] Belanger D P, King A R and Jaccarino V 1982 *Phys. Rev. Lett.* 48 1050